

Red Sequence Cluster Finding in the Millennium Simulation

J.D. Cohn¹, A.E. Evrard², M. White^{3,4}, D. Croton⁴, E. Ellingson⁵

¹*Space Sciences Laboratory, Univ. of California, Berkeley*

²*Departments of Physics and Astronomy and MCTP, Univ. of Michigan*

³*Department of Physics, Univ. of California, Berkeley*

⁴*Department of Astronomy, Univ. of California, Berkeley*

⁵*Department of Astrophysical and Planetary Sciences, Center for Astrophysics & Space Astronomy (CASA), Univ. of Colorado*

11 April 2019

ABSTRACT

We investigate halo mass selection properties of red-sequence cluster finders using galaxy populations of the Millennium Simulation (MS). A clear red sequence exists for MS galaxies in massive halos at redshifts $z < 1$, and we use this knowledge to inform a cluster-finding algorithm applied to $500 h^{-1}$ Mpc projections of the simulated volume. At low redshift ($z = 0.4$), we find that 90% of the clusters found have galaxy membership dominated by a single, real-space halo, and that 10% are blended systems for which no single halo contributes a majority of a cluster’s membership. At $z = 1$, the fraction of blends increases to $\sim 20\%$, as weaker redshift evolution in observed color extends the comoving length probed by a fixed color cut. Other factors contributing to the high- z increase include broadening of the red sequence and increased confusion from a larger number of intermediate mass halos hosting bright red galaxies of magnitude similar to those in higher mass halos. We show that a bimodal, log-normal model describes the halo mass selection function $p(M|N_{\text{gal}}, z)$ of the simulation, with a dominant component that reproduces well the real-space distribution and a redshift-dependent tail that is broader and displaced by a factor ~ 2 lower in mass. We discuss implications for X-ray properties of optically selected clusters and for cluster-finding in future, deep optical surveys.

Key words: cosmology: clusters of galaxies, large scale structure

1 INTRODUCTION

The abundance and distribution of massive dark matter halos provide a sensitive probe of cosmology and theories of structure formation. The galaxies within these halos also have their evolution strongly affected by their hosts. Clusters of galaxies are the observational realization of such halos which has inspired multi-wavelength campaigns to find and characterize them. With the advent of large format CCD cameras on large telescopes, which can find and characterize galaxies to high redshifts over wide fields, there has been renewed interest in optical searches for clusters using multicolor imaging (Kaiser et al 1998; Lubin et al 2000; Gladders & Yee 2000, 2005; Gladders et al 2006; Miller et al 2005; Koester et al 2007), see Gal (2006) for a review of optical cluster finding methods. In particular, methods which identify the cluster red sequence (Bower, Lucey, & Ellis 1992; Lopez-Cruz 1997; Gladders & Yee 2000; Lopez-Cruz, Barkhouse & Yee 2004; Gal, Lubin & Squires 2005; Gladders & Yee 2005; Gladders et al 2006; Wilson et al 2006) have attained sig-

nificant success¹ in identifying cluster candidates over wide fields to $z \simeq 1$ and above.

Because red sequence galaxies dominate the cluster population, including the reddest galaxies at a given redshift and becoming redder with increasing redshift, the restriction to red sequence colors approximately isolates a redshift slice. This redshift filtering increases the signal-to-noise of cluster detection by largely eliminating projection effects from unassociated structures along the line of sight. However, contamination is still expected from blue galaxies at even higher redshift than the cluster and from galaxies near enough to the cluster to lie within the narrow, red-sequence color region. This residual contamination is the focus of this work.

We are motivated by current red sequence based cluster searches, such as the SDSS (Miller et al 2005; Koester et al 2007), in particular by those using two filters only such as the

¹ For up to date information about the RCS and SpARCS surveys see <http://www.astro.utoronto.ca/~gladders/RCS/> and <http://spider.ipac.caltech.edu/staff/gillian/SpARCS>.

RCS and the RCS-2 (Gladders & Yee 2000; Gladders et al 2006) and SpARCS (Wilson et al 2006). We investigate the nature of the cluster population selected by a two filter method. The selection is tuned to the red cluster sequence identified in mock galaxy samples of the Millennium Simulation (MS) (Springel et al 2005; Croton et al 2006; Lemson et al 2006). We use joint halo-cluster membership as a means of categorizing the purity and completeness of the cluster population. Our cluster finder is therefore patterned after the scheme used in three dimensions to identify halos. We apply a circular overdensity algorithm, centered on bright z -band galaxies, to spatial projections of the galaxy populations at the discrete redshifts $z = 0.41, 0.69$ and 0.99 . As a point of nomenclature, we shall use “clusters” to refer to objects found by the algorithm and “halos” to refer to the dark matter halos identified in the simulation using the full 3D dark matter distribution.

An advantage of the Millennium Simulation is that it provides mock clusters situated in their correct cosmological context as part of the evolving cosmic web. Including the cosmic web is significant because projections of superclusters, structures that tend to align along filaments meeting at the cluster of interest, provide a major source of confusion for cluster identification that is difficult to otherwise model. By having available the full 3D galaxy and dark matter distribution in the simulation we are able to monitor and isolate different physical effects which can influence red sequence cluster finding.

The outline of the paper is as follows. We describe our methods in §2 and give our findings for the MS in §3. We consider some implications and properties of the blends in §4 and discuss properties causing and correlating with the blending which might extend beyond our particular search algorithm and simulation in §5. We conclude in §6.

2 METHODS

The context for our study is the model of the spatial distribution of massive halos and the galaxies that inhabit them provided by the Millennium simulation (Springel et al 2005; Lemson et al 2006). This is a collisionless dark matter simulation performed in a periodic cube $500 h^{-1} \text{Mpc}$ (comoving) on a side, using 10^{10} particles for a cosmology with parameters $(\Omega_m, \Omega_\Lambda, \sigma_8, \Omega_b, h, n) = (0.25, 0.75, 0.9, 0.045, 0.73, 1.0)$. Mock galaxies, with luminosities and colors, are generated by post-processing the dark matter halo merger trees with a semi-analytic prescription for the gas dynamics and feedback. For details, see Croton et al (2006).

We focus our cluster finding investigation on local confusion, projections on spatial scales $\lesssim 250 h^{-1} \text{Mpc}$ of a target halo that will, at these redshifts, be barely resolved by photometric redshifts of the next-generation surveys (DES², CFHT-LS³, Pan-Starrs⁴, KIDS⁵, SNAP⁶, LSST⁷). We use the simulated galaxy and halo catalogues at three fixed

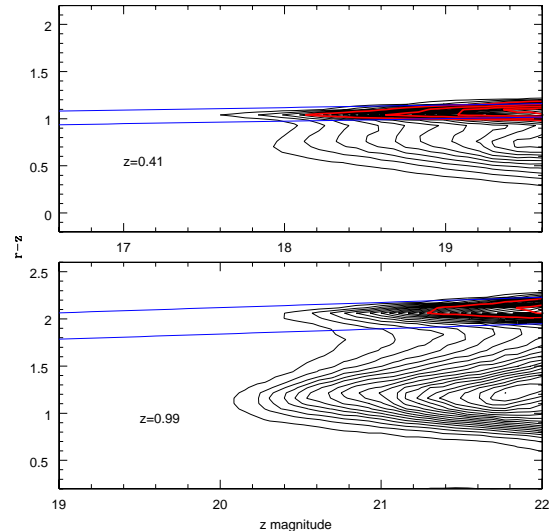


Figure 1. Top: Distributions of $r - z$ colors and magnitudes at redshifts 0.41 and 0.99 for all z -band magnitude-limited galaxies (thin line) and for those galaxies in halos with at least eight members (heavy line). Contours are in steps of ~ 600 and ~ 300 galaxies for the low and high redshifts respectively, and straight lines show the color magnitude cut applied at each redshift.

epochs given by redshifts $z = 0.41, 0.69$ and 0.99 . These values span much of the expected redshift range of interest for a survey such as the RCS. Halos in the simulation are found by using a friends-of-friends algorithm (Davis et al. 1985) and galaxy membership is determined based on this. Their masses are given in terms of M_{200c} (denoted as M henceforth), the mass enclosed within a radius interior to which the mean density is 200 times the critical density at that epoch. At our redshifts there were 1268, 805 and 426 halos with $M \geq 10^{14} h^{-1} M_\odot$ and 113, 47 and 19 halos with $M \geq 3 \times 10^{14} h^{-1} M_\odot$.

For the red sequence search, the SDSS r and z filters, which bracket the 4000 Angstrom break for approximately $0.5 \leq z \leq 1$, are employed. At the highest redshift, we also considered i band, our results for this case are described at the end of §4; results below will be given for $r - z$ unless stated otherwise.

2.1 Galaxy Colors in Massive Halos

A red sequence exists within the Millennium simulation itself over the range of redshifts probed. We define it from the simulation as follows. We take galaxies above $\sim \frac{1}{2} L_*$, corresponding to z -magnitudes of 19.6, 21 and 22, at redshifts 0.41, 0.69 and 0.99, yielding samples of 942313, 1005469 and 1054711 galaxies, respectively. For these Fig. 1 shows that a red sequence in $r - z$ vs. z exists in rich halos over the range of redshifts probed. The thin lines show the contours for the full, magnitude limited population. The colors of galaxies in halos with 8 or more members are shown by the heavy line. We fit a linear relation in the $r - z$ vs. z plane to galaxies in these latter halos which lie within $0.5 h^{-1} \text{Mpc}$ (comoving) of the known halo center. As in Gladders & Yee (2000), we throw out 3σ outliers and iterate the linear fit several times.

² <http://www.darkenergysurvey.org>

³ <http://cadwww.hia.nrc.ca/cfht/cfhtls/>

⁴ <http://pan-starrs.ifa.hawaii.edu>

⁵ <http://www.astro-wise.org/projects/KIDS/>

⁶ <http://snap.lbl.gov>

⁷ <http://www.lsst.org>

Table 1. Changes in redshifts, colors and cuts for three boxes used.

Redshift	z_{\min}	z_{\max}	intercept	slope	half-width: Δ_{\perp}	$\frac{d(r-z)}{d(h^{-1}\text{Gpc})}$ low/high	$\frac{dz-\text{mag}}{d(h^{-1}\text{Gpc})}$ low/high
0.41	0.31	0.51	0.56	0.027	0.072	-0.72/ 1.30	-0.56/0.52
0.69	0.57	0.81	0.79	0.049	0.12	-1.10/0.36	-0.80/0.64
0.99	0.85	1.14	0.88	0.055	0.14	-0.40/0.72	-1.08/1.40

Change in redshift across the Millennium box at different redshifts, red sequence intercept and slope, half-width of color-magnitude cut (Δ_{\perp}), the $r-z$ color change across the box (to front, and then to back, per h^{-1} Gpc), and the z magnitude change across the box. Color and magnitude changes are taken from the Bruzual-Charlot (2003) model as described in the text, see also Fig. 2a.

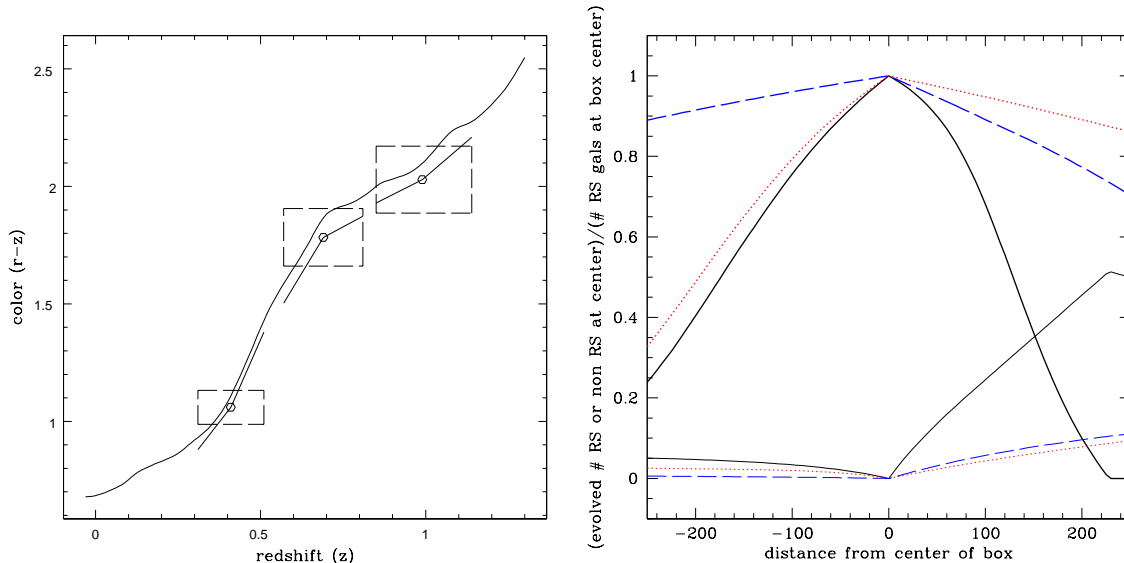


Figure 2. **Left:** Solid lines show the $r-z$ color evolution of a $z=3$ burst population synthesis model Bruzual & Charlot (2003). Sloped solid line segments show the color gradients, listed in Table 1, that we apply when projecting the galaxy population along a line-of-sight. Circles show the mean colors of the MS red sequence galaxy members. Vertical portions of the dashed boxes at each epoch mark the foreground and background redshifts of the $\pm 250 h^{-1}$ Mpc volume, while the horizontal lines mark the approximate range of color within the red sequence at each redshift. **Right:** The relative fraction of galaxies remaining on the red sequence as a function of projected distance (heavy lines). Solid, dotted, and dashed correspond to $z = 0.41, 0.69$ and 0.99 , respectively. The width of this peak controls the redshift range of galaxies selected with the red sequence. Thin lines give the relative number of non-red sequence galaxies that move into the red sequence as their observed color and magnitude vary due to their line-of-sight displacement. All counts are normalized by the number of red sequence galaxies present at the (unshifted) center of the box.

The resulting red sequence parameters are shown in Table 1 where $r-z = [\text{slope}] * z + [\text{intercept}]$. A galaxy is considered a member of the red sequence if it falls within the distance enclosing 90% of the galaxies within $0.5 h^{-1}$ Mpc (comoving) of the centers of halos with 8 or more galaxies. The distance Δ_{\perp} is taken to be the perpendicular to the red sequence line on the color magnitude plot. Table 1 lists the slopes, intercepts and distance cut from the red sequence for all 3 redshifts in z -magnitude and $r-z$ color. The red sequence color-magnitude relation is a weak function of halo mass or richness. Defining the red sequence from the MS itself means that our color cut is consistent with our rich halo definition.

Note that we used our privileged information concerning the halos and their occupants in the simulation to define the red sequence and tune the cut to keep the majority of the red sequence cluster galaxies. This is thus a best case estimate. In reality one would have to derive these cuts from the data self-consistently, as done by e.g., Gladders et al (1998) and Koester et al (2007). Comparing the simulation results to observations it appears that the mock red sequence is slightly wider than the observed one. We experimented with “tightening” the red sequence by moving the galaxy colors closer to the best-fit line, but such a procedure did not have a large effect on our conclusions so we present our results using colors as provided.

Our cluster finding depends on the red sequence defined as above from the simulation itself, and the relative change in color from evolution with redshift. Starting with the co-eval MS galaxy samples, we introduce passive evolution into spatial projections to mimic the behavior of a light-cone population. The color evolution with redshift is based on an instantaneous Bruzual-Charlot (BC) burst at $z \approx 3$ and shown for $r - z$ in Fig. 2a.⁸ For comparison, we show the average (slightly bluer) color of the MS red sequence galaxies for our three redshifts. The MS red sequence galaxies are expected to be bluer than the BC model, since their stars were not formed in a single burst at high redshift. The MS galaxies are also bluer than BCG's in the SDSS (Bernardi et al 2007).

We use this simple BC model to define piecewise constant color gradients, $d(r - z)/d\text{redshift}$, along the line of sight, shown in Fig. 2a. We define a z magnitude gradient analogously. Foreground and background color-magnitude evolution are modeled separately, with parameters given in Table 1. For $r - z$ color, these gradients are shown graphically by the line segments in Fig. 2a. Note that the color gradient becomes progressively shallower at higher redshift.

We apply these gradients in observed galaxy color and magnitude to all galaxies along the projected line of sight to build approximate light cone segments. Fainter galaxies may evolve into the z magnitude cut because of the change in observed magnitude with redshift. To catch these potential interlopers, we employ galaxy catalogues half a magnitude fainter in z -band than required by the unevolved red sequence cuts. The assumed degree of color and magnitude evolution is key since it controls the redshift filtering power of the red sequence.

To foreshadow one of our main results, Fig. 2a illustrates how projected colors vary with projected distance and how that variation affects the fraction of galaxies found to lie on the red sequence. The dashed regions in Fig. 2a are centered at the average color of the red sequence galaxies at each redshift and are bounded vertically by the approximate range of color of the red sequence. They are bounded horizontally by the redshift extents of the comoving $\pm 250 h^{-1}$ Mpc sightline available within the MS volume. At $z \approx 0.41$, the evolutionary color gradients are strong enough that projected red sequence galaxies will shift out of the target color range before the $\pm 250 h^{-1}$ Mpc MS boundary is reached, but this is not quite the case at $z \approx 0.69$ and 0.99 .

Fig. 2b shows how the imposed redshift evolution acts as a redshift filter. We take the color and magnitude of each galaxy lying in the red sequence and use our line of sight gradients to find their counterparts if that galaxy is shifted towards or away from the observer by the distance shown. Fig. 2b shows the fraction of these galaxies remaining within the red sequence as a function of projected distance. These remaining galaxies will still be potential members of a cluster centered at the origin. A more narrowly peaked distribution indicates a smaller fraction of galaxies available for inclusion via projection during cluster finding. As can be seen, the fraction of galaxies remaining within the red se-

quence cut at large distances from the origin increases with redshift; the red sequence selects a longer path along line of sight at higher redshift.

The other source of contamination is galaxies that are shifted into the red sequence by the change in observed color. The number density of these galaxies, normalized by the number of red sequence galaxies at the box center, is shown by the light lines in Fig. 2b. Except for the most distant part of the box at $z = 0.41$, this number is relatively small. Our use of a uniform color change with redshift for all galaxies is not strictly correct for all galaxy types. However, blue star forming galaxies change in observed color much more slowly with redshift than in this model, so to be shifted erroneously into our red sequence color cut, these galaxies are required to be at significantly higher redshift than the cluster. Since they would then lie outside of our $500 h^{-1}$ Mpc box, they are not included in our analysis. The strongest contribution to interloper candidates is from galaxies which have colors within our red sequence color cut even though they are far from the central galaxy along the line of sight.

2.2 Cluster Finding Algorithm

Our algorithm defines clusters as circular regions of fixed, red-sequence sky surface density equal to some multiple Δ_p of the mean. We work in descending order through a list of red-sequence galaxies ranked (brightest to dimmest) by apparent z -band magnitude. This ranking is motivated by a desire to find the rare, high mass halos first, then work down the mass function to more common objects.

Around a potential cluster center, a radially-sorted list of red sequence neighbors is used to define a mean galaxy number density profile as a function of transverse separation. We use the periodic boundaries of the MS to recenter the simulated volume on each candidate center. The box extends $250 h^{-1}$ Mpc in front and behind, and galaxy colors are adjusted, linearly with distance in the projected direction, as described above. We define N_{gal} and r_{gal} as the largest values that satisfy the overdensity criterion

$$\Delta \equiv \frac{N_{\text{gal}}}{\bar{n}\pi r_{\text{gal}}^2} \geq \Delta_p, \quad (1)$$

where \bar{n} is the mean sky surface density of red sequence galaxies. This mean sky density includes the effects of the applied color evolution along the projected dimension. If N_{gal} meets or exceeds a minimum of 8 galaxies, then this cluster is added to the output list. All members are then recorded and removed from the remaining list of potential cluster centers.⁹ Note that area overlap of clusters is allowed,

⁸ We thank N. Padmanabhan and B. Koester for the evolution of galaxy colors using Bruzual & Charlot (2003) as in Padmanabhan et al (2006).

⁹ The choice of Δ_p , a parameter in the cluster finding, is discussed below. Roughly the cluster will have a density of red sequence galaxies Δ_p times the average red sequence (background) density, $\sim 0.7/(h^{-1} \text{ Mpc})^2$ in our case. The approximate change of radius with richness can be read off from Eq. 1. Note too that our cluster-finding algorithm traces galaxy overdensities to radii which can potentially reach greater than $1 h^{-1}$ Mpc. This algorithm increases the survey sensitivity to truly extended structures, but may also increase the cross-section for interlopers relative to algorithms which search for clusters only on a limited, smaller scale. We found that a fixed aperture richness based cluster finder performed significantly more poorly, however.

so that a single galaxy can belong to more than one cluster. To boost statistics, we make three projections of the simulated volume along its principal axes. The choice of Δ_p is discussed below.

2.3 Cluster-Halo Matching

The clusters found by the search algorithm can be linked back to the dark matter halos in the simulation using their respective lists of galaxy members. A perfect algorithm would be complete with respect to halos and have no false positives, *i.e.*, no clusters that appear rich on the sky which are actually several less rich systems aligned along the line-of-sight. In addition, the halo and cluster richnesses would agree. A perfect algorithm would therefore recover the intrinsic distribution of halo mass M as a function of red sequence galaxy richness N_{gal} . This distribution is shown in the top panels of Fig. 3.

At all redshifts, a mean richness of $N_{\text{gal}} \simeq 20$ above our z -magnitude limit corresponds to a $\sim 10^{14} h^{-1} M_{\odot}$ halo. When fit above a minimum of 8 members, we find that mass scales with red sequence richness as $M=M_{20}(N_{\text{gal}} - 1)^{\alpha}$, with $\alpha = 1.04, 1.11$ and 1.15 at $z=0.41, 0.69$ and 0.99 respectively. The mass intercepts are $M_{20}=1.3, 1.4$ and $1.6 \times 10^{14} h^{-1} M_{\odot}$ and there are $\sim 3900, 2700$, and 1100 $N_{\text{gal}} \geq 8$ halos at these redshifts, respectively. Note that red sequence richness is a fairly noisy tracer of mass; the rms level of scatter is $\sim 50\%$ or higher above the richness cut of $N_{\text{gal}}=8$ (a detailed discussion of scatter in richness vs. mass can be found in White & Kochanek (2002); Dai, Kochanek & Morgan (2007)). The richness we use in finding the clusters may not be the best richness to use for getting the cluster mass (e.g. galaxy counts within some aperture might be useful after the clusters are found, for finding the clusters themselves we found a fixed aperture performed significantly worse). Some observational surveys for galaxy overdensities account for projections of foreground/background galaxies via a statistical subtraction of the expected number of projected galaxies, calculated from random non-cluster pointings. Our cluster richness estimator, N_{gal} , does not include such a correction; our overdensity requirement means that approximately $1/\Delta_p$ of the galaxies are from the background.

For each cluster identified in projection, we list all halos contributing one or more of its member galaxies. The quality of the cluster detection is measured by the top-ranked matched fraction, f_{1h} , defined as the fraction of cluster members coming from the halo that contributes the plurality of the cluster's red sequence galaxies. We define two classes, *clean* and *blended*, based on whether the plurality is or is not the majority of the cluster's membership,

$$\text{clean} : f_{1h} \geq 0.5, \quad (2)$$

$$\text{blended} : f_{1h} < 0.5, \quad (3)$$

We assign to each cluster the mass of its top-ranked halo found through member-matching. If two (or more) halos contribute the same number of galaxies, and are both top-ranked, we take the most massive.

3 RESULTS

An ideal cluster catalog would be *pure*, *complete* and *unbiased* with respect to halos. A perfectly *pure* sample would have no accidental projections; all the galaxies of any chosen cluster would be common members of a single, dark matter halo. A perfectly *complete* sample would be one for which each halo in the survey volume appears once, and only once, in the list of clusters. Finally, an *unbiased* cluster catalog would contain clusters that reproduce the mean mass-richness relation defined by halos. In this section, we consider these issues, both in the context of setting our circular overdensity threshold and in the results obtained. We will see that high levels of purity and completeness are achieved, and that the cluster samples are nearly unbiased.

3.1 Cluster finder threshold and two examples

The cluster catalogs produced by the search algorithm depend on the value of the number density threshold Δ_p . Choosing too high a value will pick out only the cores of the richest halos, resulting in a catalog that is pure and complete at very high masses, but is otherwise incomplete. Picking too a low value will extend the search into the periphery of halos, leading to a catalog that, although complete across a wide range of masses, suffers from impurities due to blending multiple halos into a single cluster. Our interest is in obtaining roughly the maximum number of clean clusters, which informed our choice (other tradeoffs between purity and completeness might be chosen if one was creating a catalogue for e.g. X-ray follow up). After some experimentation we found that $\Delta_p = 7$ was a good compromise between completeness and efficiency for all three redshifts, for the richness values of interest ($N_{\text{gal}} \sim 20$) and thus used it for simplicity¹⁰. The fraction of halos found for each halo richness with this choice is shown in Fig. 4; increasing Δ_p decreases these fractions although it reduces blending.

With $\Delta_p = 7$ the cluster catalogs have on average (for the three projections) 3909, 2468 and 1030 clusters with $N_{\text{gal}} \geq 8$ at $z = 0.41, 0.69$ and 0.99 , respectively (distributed in richness according to Fig.5, also shown are the MS halo numbers which are 3898, 2691, 1154 for $N_{\text{gal}} \geq 8$). These cluster numbers are within 10% of the number of halos with the same richness at those redshifts, however the good match does not imply that the algorithm is perfect. In fact the typical number of halos contributing to an $N_{\text{gal}} \geq 8$ cluster is $\sim N_{\text{gal}}/4$ (slightly more at the highest redshift). The mass distribution of clusters and halos with one given richness can be seen below, in Fig. 7 in section 3.2.

The second and sixth richest clusters found at $z = 0.41$ illustrate the range of behavior of clean and blended clusters. Figure 6 shows projected positions and color-magnitude information for sky patches centered on the two clusters. The second richest cluster has 204 members contributed by 23 different halos. Members of one of the most massive halos at that epoch, $M = 2.0 \times 10^{15} h^{-1} M_{\odot}$, comprise 87% of the cluster members. The remaining members come from

¹⁰ Slightly higher Δ_p for the two lower redshifts gave a slight improvement, but cut completeness severely in our target richness range for $z = 0.99$. Optimizing Δ_p at each redshift separately to find the largest number of clean clusters gives similar results.

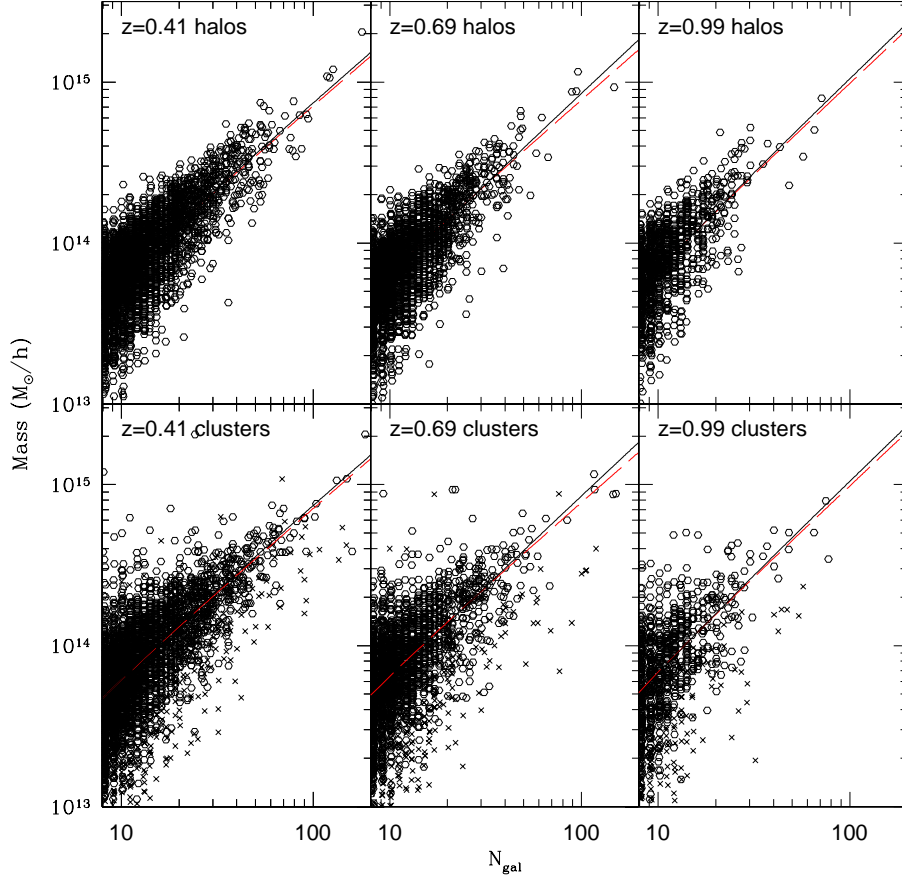


Figure 3. Top: relation between halo mass and red sequence galaxy richness at $z=0.41, 0.69$, and 0.99 (left to right). Bottom: relation between cluster mass and red sequence galaxy richness at the same redshifts, taken along one projection axis. Crosses have $f_{1h} < 0.5$ and comprise (10%, 13%, 18%) of the $N_{\text{gal}} \geq 8$ clusters. Solid (dashed) lines are least-squares fits for $N_{\text{gal}} \geq 8$ halos (clean clusters).

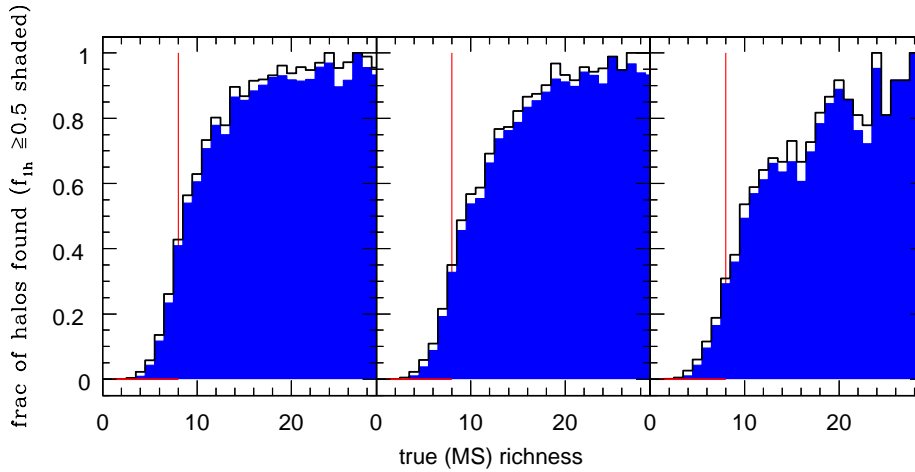


Figure 4. Completeness for our choice $\Delta_p = 7$ for overdensity. Fraction of halos found as a function of halo richness, solid line is fraction found in any cluster, shaded region is fraction found in a clean ($f_{1h} \geq 0.5$) cluster. Left to right is redshift 0.41, 0.69, 0.99 respectively. Vertical line is minimum cluster apparent richness imposed ($N_{\text{min}} = 8$); if true and apparent richness were identical no clusters would be found to its left.

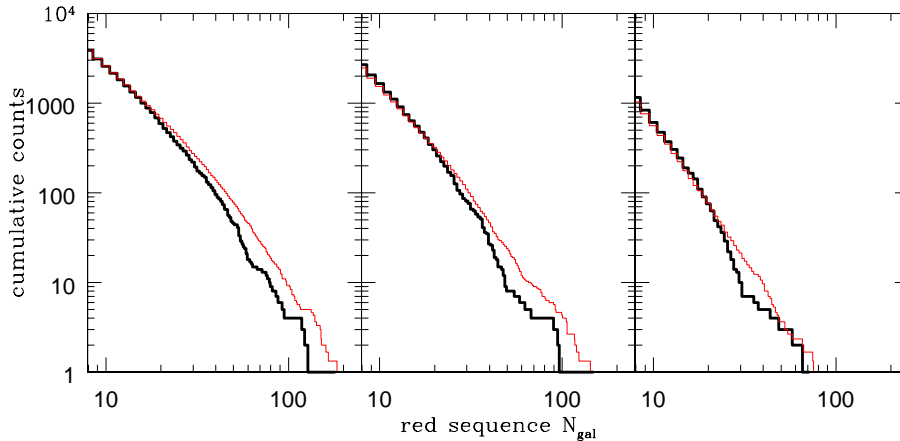


Figure 5. Cumulative number of halos as a function of red sequence richness N_{gal} (bold) compared to the average number of clusters found using the circular overdensity method applied to three projections of the galaxy samples (light).

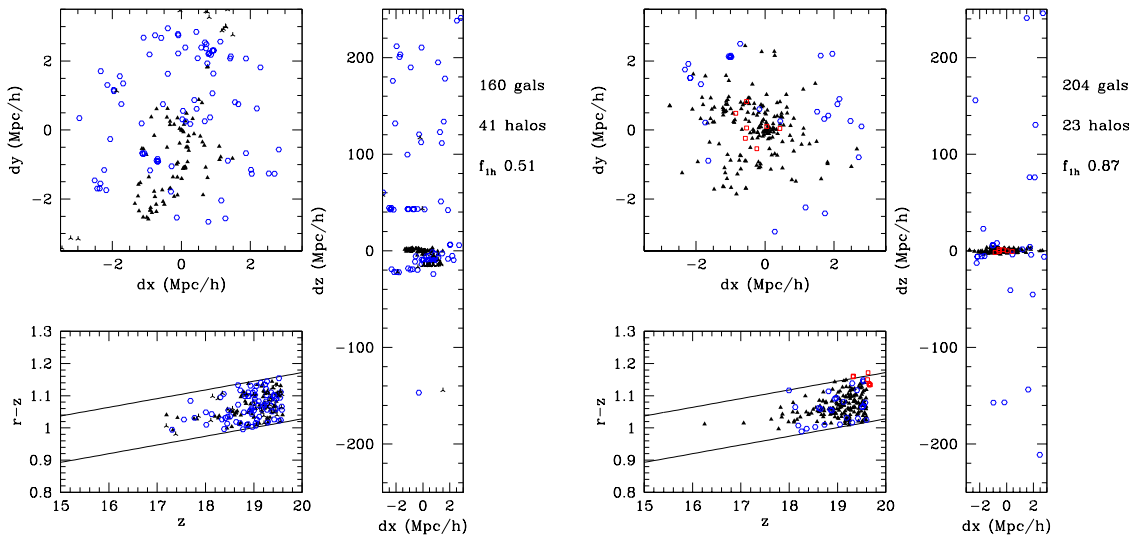


Figure 6. Examples of blended (left) and clean (right) rich clusters found at $z=0.41$. Filled triangles are members of the first-rank matched halo, open circles are other cluster members. Open squares are members of the best fit halo not in the cluster. Stars towards e.g. the top of the lefthand figure are members of the red sequence not in the found cluster. Comoving scales are shown, note that the axes in the dz vs. dx figure are scaled differently.

22 other halos, including some lying in the foreground. A small number of members are contributed by halos in the background.

The sixth richest cluster, with 160 members, presents a very different case. Its most massive contributing halo has a mass $M = 3.8 \times 10^{14} h^{-1} M_{\odot}$, which contributes almost all of its own galaxies but only 50% of the cluster's members ($f_{1h} = 0.50$), making it barely a clean cluster by our definition. A total of 40 other halos also contribute, from halos lying $\lesssim 30 h^{-1}$ Mpc in the foreground to $250 h^{-1}$ Mpc in the background. There is also an isolated galaxy far into the foreground.

Although much richer than most of the halos consid-

ered, these two examples illustrate the essential projection problem that is causing the blends; both sets of galaxies appear to be reasonable clusters in the x - y plane. In the next two sections the statistics of the clean and blended clusters, and their features, will be discussed in more detail.

3.2 Mass selection function of clusters

At all redshifts, the circular overdensity algorithm is effective at identifying the underlying population of massive halos. The bottom row of Fig. 3 shows the relationship between observed cluster richness and top-ranked halo mass (see § 2.3). Circles show clean clusters while small crosses

show blends. At each redshift, the clean cluster population displays a slope similar to, but slightly flatter than, that of the underlying halo population. Slopes of halos (clean clusters) for $N_{\text{gal}} \geq 8$ are 1.04 (1.02), 1.11 (1.04), 1.15 (1.11) from low to high redshift, respectively. The intercepts could be fine-tuned via small changes to the search threshold Δ_p , but this behavior is insensitive to this detail.

Normalized cross-sections of the data in Fig. 3 give the conditional halo mass distribution, $p(M|N_{\text{gal}}, z)$, an important ingredient for cosmological tests with optical cluster surveys (White & Kochanek (2002), see also the formalism developed in Rozo et al (2007)). We show this likelihood in Figure 7 for a richness range that gives the same average halo mass, $1.2 \times 10^{14} h^{-1} M_{\odot}$, at all 3 redshifts: $N_{\text{gal}} = (18, 18, 16) \pm 4$ at redshifts (0.41, 0.69, 0.99).

The cluster likelihoods (shaded in the figure) are compared with the halo distributions for the same richness ranges, shown by solid lines. The top row shows all clusters, while the middle and bottom rows separate the samples into clean and blended systems, respectively. Raw counts rather than normalized likelihoods are shown to give the number of objects.

At $z \approx 0.41$, more than 90% of clusters in the chosen richness range have their dominant underlying halo contributing at least half of the galaxies. The mass distribution of the found clusters matches well the underlying halo mass likelihood; both have the same mean, $\sim 1.2 \times 10^{14} h^{-1} M_{\odot}$.

At higher redshift, going to the right in Fig. 7, the correspondence between halos and clusters weakens somewhat; the number of blends nearly doubles, from 10% at $z \approx 0.41$ to 18% at $z \approx 0.99$. The blended systems contribute a low mass tail to the halo mass likelihood. For the distributions, the central mass of the clean clusters remains around $1.2 \times 10^{14} h^{-1} M_{\odot}$ at all 3 redshifts, while the central mass of the blends drops, from $6.5 \times 10^{13} h^{-1} M_{\odot}$ at $z = 0.41$ to $5.5 \times 10^{13} h^{-1} M_{\odot}$. Thus the ratio of central masses between the clean and blended clusters also increases with redshift.

Our classification of clean versus blended clusters is based on a somewhat arbitrary cutoff of 0.5 in member fraction. Figure 8 provides a more complete picture by plotting the cumulative fraction of the clusters shown Fig. 7) that have top-ranked halo member fraction $< f_{1h}$. There is a clear trend with redshift, with clusters at $z \approx 0.99$ being less well-matched to halos than those at $z \approx 0.41$. The median value of f_{1h} tells a similar story, decreasing from ~ 0.8 at $z \approx 0.41$ to ~ 0.7 at $z \approx 0.99$. Blending is clearly increasing at larger redshift.

Going to a higher central mass gives similar trends, e.g. centering on a richness corresponding to a average $1.6 \times 10^{14} h^{-1} M_{\odot}$ halo mass at all redshifts gives a clean fraction of 87% at redshift 0.41 which decreases to 73% at redshift 0.99 for the same Δ_p as above (Δ_p can be increased for higher richness to improve both numbers but the increase of blends at high redshift remains).

3.3 Causes and trends for blends

There are several effects which cause an increasing incidence of blends at higher redshift. Firstly, the change of observed color with distance is weaker, and secondly, the red sequence is wider, so the color-magnitude cut selects galaxies from a

[htb]

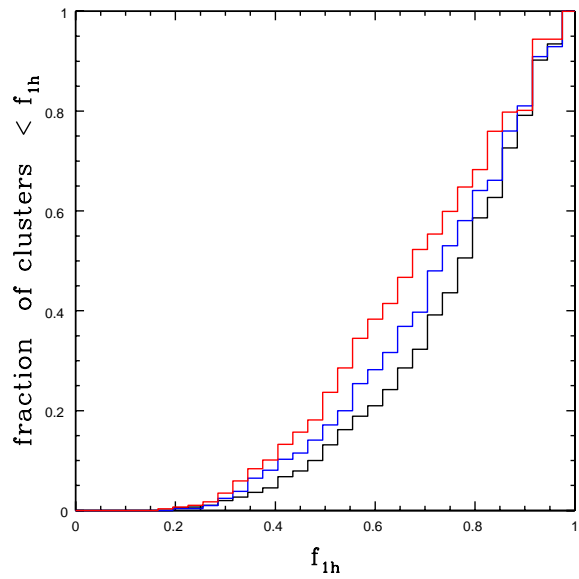


Figure 8. Cumulative fraction of clusters in Fig. 7 as a function of the top-ranked halo fractional member contribution, f_{1h} . Top to bottom lines are redshifts, $z \approx 0.99, 0.69$ and 0.41 . The fraction of galaxies from the top-ranked halo declines with increasing redshift.

thicker slice along the line of sight. These seem to be the strongest causes and were illustrated in Fig. 2.

Another way of seeing the effect of color/magnitude evolution is to remove it entirely at $z = 0.41$; the background level then increases and the contrast between the clusters and the background declines. Lowering Δ_p to obtain the same number of clean clusters at the fixed mass range of Fig. 7, we find that the level of blends increases to $\sim 20\%$, very close to what is seen at $z \sim 0.99$. Similarly, to increase the clean fraction, one can impose the $z = 0.41$ color evolution on the $z = 0.99$ box, again fixing true halo mass and number of clean clusters (by changing Δ_p). (However, in this case the number of non-red sequence galaxies brought into the red sequence through our evolution increases strongly, limiting how much the blends can be reduced.)

A third contributing factor is that at earlier times, the mass function is steeper, meaning the number of possible interloper halos per target halo (of mass $\sim 10^{14} h^{-1} M_{\odot}$, for example) is larger at high redshift. The increase in intermediate-mass halos is also enhanced because the central galaxy magnitude is less well correlated with host halo mass at $z \approx 0.99$ than at low redshift. Over time, central galaxies in massive halos grow and brighten via mergers, leading to a stronger correlation between z -magnitude and mass. Our cluster finding algorithm works in descending order of luminosity, so, at high redshift, it needs to sift through more low mass systems before finding all of the high mass halos.

The trend toward more blends at $z \approx 0.99$ appeared in all the cases we considered: changing definition and tightness of the red sequence, changing N_{gal} cuts and changing the spherical overdensity requirement. For a wide range of density cuts and modeling choices the blends have roughly half

[htb]

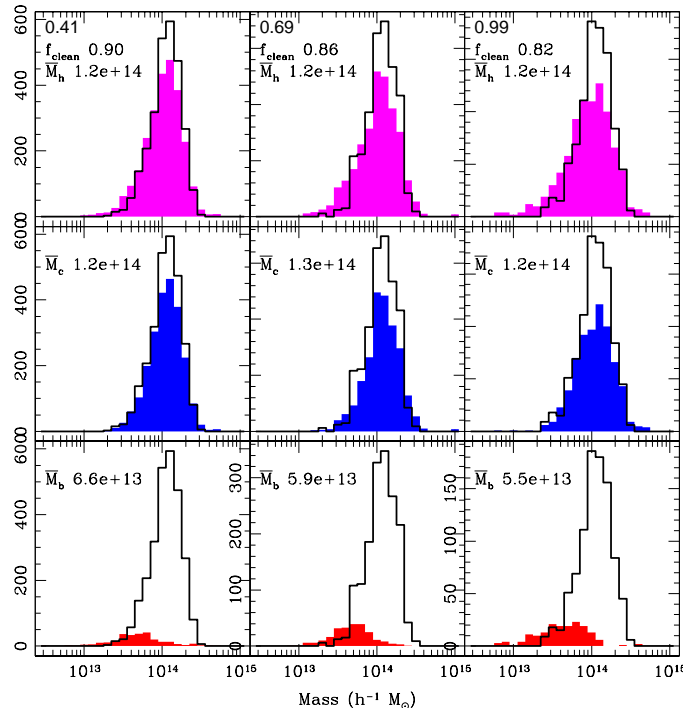


Figure 7. Mass selection functions $p(M|N_{\text{gal}})$ with richness $N_{\text{gal}} = (18, 18, 16) \pm 4$ at redshifts $z = (0.41, 0.69, 0.99)$ (left to right). Solid lines give the intrinsic halo mass distribution, and are the same in each column. The shaded distribution in the upper row gives $p(M|N_{\text{gal}})$ for clusters found with $\Delta_p = 7$. The middle row shows $p(M|N_{\text{gal}})$ for clean clusters ($f_{1h} \geq 0.5$) while the bottom row gives the mass distribution of blended clusters ($f_{1h} < 0.5$). The bottom and middle shaded regions add up to the shaded region in the top panels. The average mass of the halos/clean clusters/blended clusters are shown respectively in the top/middle/bottom panels for each redshift. The fraction of clean clusters f_{clean} is also shown for each redshift.

Table 2. Expected Cluster X-ray Properties.

Redshift	$\langle L \rangle_{\text{halo}}^a$	$\langle L \rangle_{\text{clean}}^a$	$\langle L \rangle_{\text{blends}}^a$	f_{blends}
0.41	1.4 (0.96)	1.6 (1.0)	0.70 (1.4)	0.10
0.69	1.5 (0.95)	1.8 (1.0)	0.59 (1.2)	0.16
0.99	2.0 (0.95)	2.0 (1.1)	0.62 (1.3)	0.20

^a Numbers in parenthesis give the log-normal scatter, $\sigma_{\ln L}$.

the mass of the clean matches at $z = 0.41$, and this mass scale declines at higher redshift.

4 IMPLICATIONS

Since blended clusters are associated with lower mass halos, they will be evident in follow-up studies as such. Their mean lensing signal, X-ray luminosity and temperature, and thermal SZ decrement should be low relative to clean systems. Spectroscopic signatures of substructure, in the form of multiple peaks or other departures from Gaussianity, would also be likely in these systems. The imprecise centering of the multiple components along the line-of-sight would tend to flatten the radial number density profile.

Table 2 provides estimates of the soft band X-ray lumi-

nosity from our MS blended and clean clusters with richness 18 ± 4 (now fixed across redshifts), compared to values for halos of the same richness. We assume a power-law relation of the form $L = (M/10^{14} h^{-1} M_{\odot})^{1.6}$ (Stanek et al 2006), and quote values normalized, arbitrarily, to the luminosity of a $10^{14} h^{-1} M_{\odot}$ halo at each epoch. We also assume scatter in the mass-luminosity relation, $\sigma_{\ln M} = 0.4$, and combine this with the dispersion in mass for the chosen richness range (Fig.7) to give the dispersion in luminosity, $\sigma_{\ln L}$. Lower values have been suggested for $\sigma_{\ln M}$ (Reiprich & Boehringer 2002), but the scatter in mass at fixed N_{gal} dominates the intrinsic L-M scatter anyway.

The clean clusters have mean X-ray luminosities that tend to be slightly higher than the corresponding values for halos of the same richness. The blended systems are substantially dimmer. At $z = 0.41$, the 10% of the cluster population that are blends have mean luminosity equal to half the value of correspondingly rich halos. At $z = 0.99$, the behavior gets more extreme, with 20% of the population having, on average, less than one-third of the luminosity of halos.

Instead of using only the top-ranked halo mass to determine the X-ray signal, we can instead sum the luminosity of all contributing halos. In this case, all the cluster luminosities go up, with the clean subset increasing by roughly 20% and the blended subset increasing by a larger amount. Then

the ratio of clean to blended mean luminosities changes to ~ 1.5 at low redshift and to slightly above two at high redshift. The luminosity measured by X-ray observation will depend on details of the projected spatial arrangement, the noise characteristics and other details that lie beyond the scope of this investigation. It seems reasonable to consider the values quoted for the single halo case as a lower bound, and the values from summing all halos as an upper bound, on what would be observed.

The existence of blends should be a generic outcome of red sequence-based cluster finding methods, and there are indications of this from initial X-ray and dynamical observations of the RCS clusters. In Chandra observations of 13 clusters at $0.6 < z < 1.0$, Hicks et al (2005, 2007) confirm 12 as X-ray sources at $3\text{-}\sigma$ significance, suggesting that $> 90\%$ of the cluster candidates are massive structures with deep gravitational potential wells (see also Blindert et al (2007)). However, their X-ray luminosities were systematically lower at a given cluster richness than seen for lower-redshift X-ray selected clusters. Most of the clusters lay on a sequence only slightly offset from the expected L_x -richness relation, but several clusters were significantly offset. Optical spectroscopy of one of these clusters (at $z=0.9$) showed that it consisted of several structures which are dynamically discrete but whose red sequences were overlapping in the survey data (Gilbank et al 2007)– precisely the sort of blended system expected by the study here. Evidence for large scatter between X-ray luminosity and optical richness has been seen in e.g. Yee & Ellingson (2003); Gilbank et al (2004); Hicks et al (2005); Barkhouse et al (2006).

Another difference between clean and blended systems is in their radial cluster profiles. Stacked profiles of the clean and blended clusters are used to produce the density profiles, $\rho(r) = \frac{1}{N_{clus}} N(r)/(r^2 dr)$, shown in Fig. 9. The clean clusters have a significantly steeper mean density profile than the blends. This result suggests that a matched angular filter approach (Postman et al 1996) could offer improvements, particularly one that includes radial distance information from photometric redshifts or colors (White & Kochanek 2002). Observations of colors with distance to cluster center (e.g. Ellingson et al (2001); Blindert et al. (2004)) and other properties (e.g. De Lucia et al (2004)) are already in place at high redshifts. Going further down the luminosity function would provide more galaxies to trace out the profile, but at the risk of including more faint background galaxies redshifted into the color region.

The interlopers in both clean and blended clusters, as expected by Gladders & Yee (2000), lie (slightly) more frequently in the background than the foreground. There doesn't seem to be a strong trend in the moment of inertia for clean versus blended clusters; often the blends are projections, rather than objects which are merely unrelaxed.

We also considered using $i - z$ color at high redshift, rather than $r - z$, and found a similar blend fraction, even though the red sequence turns out to be narrower. This is because the evolution of red sequence galaxies (now defined with respect to $i - z$) remains very slow with redshift, thus, as with $r - z$ color at high redshift, many of the galaxies do not evolve out of the red sequence even when far from the cluster center. Similarly, the number of non-red sequence galaxies evolving into the selection window remains small across the $\pm 250 h^{-1}$ Gpc projected length.

[htb]

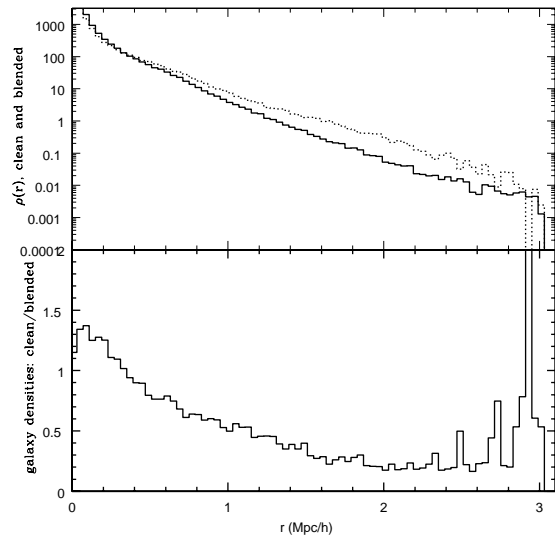


Figure 9. “Stacked” profiles of clusters with $f_{1h} \geq 0.5$ divided by those with $f_{1h} < 0.5$ for the $\Delta_p = 7.0$ case and $z = 0.41$. The case here is representative, the trend of ratio with radius was seen in all redshifts and color cuts. Stacking after rescaling by the outer radius gave similar results.

As mentioned earlier, blends can be immediately reduced by increasing the spherical overdensity criterion Δ_p , but only at the cost of losing true halos as well. An increase in Δ_p also shifts the mass-richness relation to lower values of N_{gal} compared to the intrinsic case, and decreases the number of clusters found at fixed N_{gal} . These trends reflect the usual tradeoff between purity and completeness for cluster samples; for more discussion see, e.g., the appendix of White & Kochanek (2002).

5 DISCUSSION

In the above analysis, we have found properties and trends for blends as a function of redshift. Some of these results depend on particular details of the Millennium Simulation and our method, and some are likely to be general.

Most of the increase in blends at $z \sim 1$ comes from the slower change of color with distance. This color change was not obtained directly from the Millennium simulation but from a simple stellar population synthesis model that reproduces observations. We expect this result to be general. Our implementation of the color change with redshift is crude but the candidate high redshift interlopers are mostly red sequence galaxies, where our approximation is best expected to hold. As a result, we do not expect more detailed color implementations, such as mock light cones (e.g. Kitzbichler and White (2007) for the MS), to produce substantially different local ($\pm 100 h^{-1}$ Mpc) projected contamination.

The increased width of the red sequence at high redshift is derived from the Millennium Simulation. However, at $z=0.99$, the weak color evolution combined with the deep “green valley” separating the red and blue populations in the

MS means that our results are reasonably insensitive to the precise width. Most of the interloper galaxies are themselves members of the red sequence in their respective projected halos. The $r - z$ color shift for $\pm 250 h^{-1}$ Mpc projection at $z = 0.99$ is -0.1 and $+0.18$, so only by compressing the red sequence to a width well below these values would one have an appreciable effect on the blended fraction.

The relative numbers of interloper halos at different redshifts is a property of the underlying dark matter power spectrum and linear growth rate. For a fixed target mass, more interloper halos at higher redshift are expected generically. Physically, if we look at the line-of-sight distribution of the contaminating material we find that the contaminating mass at large distances ($> 50 h^{-1}$ Mpc) more than doubles between redshift 0.41 and 0.99. This enhanced contamination from large distances is also true on a cluster-by-cluster basis: the fraction of clusters with more than e.g. 30% of their material coming from $> 40 h^{-1}$ Mpc grows significantly with redshift. This material is far outside the cluster virial radius and not just material which got “caught” by the cluster finder before it fell in to truly be part of the cluster. Note that superclusters of very large size have been seen out at these redshifts, for example see recent studies of superclusters by Gal, Lubin & Squires (2005); Nakata et al (2005).

There are other possible interlopers as well. For instance, adding galaxies that lie outside the MS volume will only increase the amount of blended contamination. Also, at faint magnitudes, the increasing numbers of background blue galaxies available to redshift into the red sequence are a potential cause for concern; increasing numbers of blue galaxies at high redshift are observed (e.g. Ellis (1997)) (it should be noted that there are observational techniques to take many of them out which we do not include here). We saw only a small fraction (except at low redshift) of candidate interlopers from galaxies outside the red sequence (cf. Fig.2). This is good, as the observed color and magnitude evolution of these galaxies was approximated to be the same as for red sequence galaxies; we expect the interloper numbers due to these objects is minimized at high redshift because of their small contribution in our approximation.

To extend our analysis of the MS (tuning the cluster finder to cluster color profiles in more detail, for example) requires further developments. The MS utilizes sophisticated physical models for properties such as star formation histories, initial mass function and stellar population synthesis models, dust production and radiative transfer models, and the sensitivity of all of these to local conditions. The resulting MS catalogues match observations of large numbers of properties (e.g. Springel et al (2005); Lemson et al (2006); Croton et al (2006)) at many redshifts. For the cluster searching here, the only properties used are the galaxy locations and their fluxes in two filters; tuning the cluster finder to properties of these fluxes (for example their trends within clusters) requires extremely high accuracy. Work is in progress to provide this accuracy as the models improve to match observations. For example, known issues in the MS under study include, for $z = 0$ clusters, a faint red satellite excess and an excess tail of bright blue objects (but with overall blue satellite fractions too low), and no “green valley” (Weinmann et al 2006a; De Lucia 2006; De Lucia et al 2007). We find a red sequence with the wrong sign for the color-magnitude slope (the brightest galaxies tend

to be slightly bluer than the fainter, see Fig. 1), and similarly the blue fraction increases towards brighter luminosity and has the wrong radial evolution within clusters for our three redshifts. In addition the simulation was run with the earlier WMAP parameters rather than the WMAP3 (Spergel et al 2006) current best fit cosmology.

Future improvements in optical cluster finding will require simulated catalogues for analysis and observed galaxy catalogues which are in more quantitative agreement at all redshifts. To refine and use more sophisticated color finders does not necessarily require all the physics employed in the MS, which aims to explain a multitude of observational properties as well as reproducing them. Mock catalogues could be based instead on e.g. halo model fits tuned to data in hand at the redshifts of interest. The catalogues can focus narrowly on observational properties relevant to the search algorithm. In particular, critical to a quantitative prediction of the amount of contamination in color-selected surveys are accurate colors for galaxies in groups and filaments in the outskirts of clusters, as red-sequence galaxies in these regions are the most likely source of interlopers. Such survey-specific catalogues are crucial to understand cluster survey selection functions, in part by allowing search algorithms to be tuned to the cluster “color footprint” and spatial profile, as has already been profitably used at low redshifts (e.g. Kochanek et al (2003); Eke et al (2004); Yang et al (2005); Miller et al (2005); Weinmann et al (2006b); Miller et al (2005); Koester et al (2007)). At high redshift, data sets large enough to tune such catalogues are just coming into being; combined with modeling improvements in recent years the construction of such catalogues is now a feasible task.

However, without such a catalogue in hand, our primary effect is still simple to illustrate. This effect is that the spatial cut provided by the observed color and magnitude cut widens as redshift increases. Conversely a narrow spatial cut reduces the blends strongly. For example, taking an exact spatial cut for the MS, boxes $100 h^{-1}$ Mpc wide at all three redshifts, the clean fraction becomes almost 100% at low redshift and 95% at high redshift. (Presumably the remaining blends are due to the other contributing factors mentioned above.) A slice this thick would correspond to a fine redshift selection, $\Delta z = 0.06(0.04)$ at redshift 0.99 (0.41). This level of accuracy is potentially attainable with next-generation photometric redshifts.

6 CONCLUSIONS

With the advent of wide field imagers, optical searches have become a powerful way to compile large samples of high redshift clusters. Key to these techniques is the use of multicolor information to reduce the line-of-sight contamination that plagued earlier, single filter, observations (Abell 1958; Dalton et al 1992; Lumsden et al 1992; White et al 1999). Two-filter information provides only limited redshift filtering, and this paper begins to explore the questions of what types of objects are selected by such techniques, and how this selection evolves with redshift.

We use a simple circular overdensity search algorithm on the Millennium Simulation, using knowledge of the red sequence present in the simulation data itself. The free parameter, the density contrast Δ_p , is tuned to maximize both

purity and completeness, and the choice $\Delta_p = 7$ produces a number of clusters as a function of galaxy richness that is close to, but somewhat shallower than, the underlying richness function of halos.

We find that essentially all clusters have some degree of projected contamination; a cluster of optical richness N_{gal} typically has red sequence members from $N_{\text{gal}}/4$ halos along the line-of-sight. In the large majority of cases, the contamination is not dominant, and most of a cluster's members are associated with a single, massive halo. A minority are highly blended cases in which projected contamination is dominant, and no single halo contributes a majority of the cluster's members.

We find an increased fraction of blends with redshift. Although several factors contribute, the most important factor appears to be weaker evolution in red sequence galaxy observed color with increasing redshift. This effectively increases the path length searched by the red sequence color cut, leading to a larger cross section for accidental, line-of-sight projections. In addition, at higher redshift, the number of $\sim 3 \times 10^{13} h^{-1} M_{\odot}$ halos relative to a $10^{14} h^{-1} M_{\odot}$ halo is larger, and the central galaxy red magnitudes at these mass scales are more similar.

The blends add a low-mass tail to the halo mass selection function for clusters of fixed optical richness. For clusters color selected in a similar way with optical richness targeting $10^{14} h^{-1} M_{\odot}$ halos, we expect that $\sim 10\%$ of these systems would be underluminous in X-rays by a factor of roughly two at $z = 0.41$, growing to $\sim 20\%$ underluminous by a factor closer to three at $z = 0.99$. The scatter in individual X-ray luminosities for the complete set of clusters is expected to be large, $\sigma_{\ln L} \simeq 1.2$ at high redshift, and there is considerable overlap in the distributions of L_X expected for clean and blended clusters.

The cluster profiles are slightly shallower for blends than for clean clusters, and a matched spatial filter approach may help identify and eliminate the former. Since some fraction of halos, those undergoing mergers especially, will also be spatially extended, careful study of the effect of spatial filtering on halo completeness is needed. Alternatively, instead of decreasing the number of blends in searches, our findings here suggest modeling the mass likelihood $p(M|N_{\text{gal}}, z)$ as a bimodal log-normal distribution, with the fraction of blends, and the location and width of that component, included as nuisance parameters.

Understanding the detailed color/magnitude trends within galaxy clusters is the key to refining red sequence cluster finding and improving its success rate. Fortunately, data sets in hand or on the way, combined with rapidly improving modeling methods, will lead to improvements in our understanding of high redshift colors and their evolution. This work will be driven largely by survey-specific mocks—current examples are the 2MASS (Kochanek et al 2003), the DEEP2 survey (Yan, White & Coil 2004), the 2dFGRS (Eke et al 2004; Yang et al 2005) and the SDSS (Miller et al 2005; Koester et al 2007; Weinmann et al 2006b) — and such efforts will be key to mining the rich science provided by existing and future high redshift cluster surveys.

JDC thanks A. Albrecht, M. Brodwin, C. Fassnacht, R. Gal, J. Hennawi, A. von der Linden, L. Lubin, G. De Lucia, S. Majumdar, T. McKay, N. Padmanabhan, R. Stanek for

helpful discussions and/or questions and the Galileo Galilei Institute and the Aspen Center for Physics for hospitality during the course of this work and the opportunity to present these results, and LBL for support. AEE thanks J. Annis and T. McKay for conversations and acknowledges support from NASA grant NAG5-13378, from NSF ITR ACI-0121671, and especially from the Miller Institute for Basic Research in Science at UC, Berkeley. DJC wishes to thank both the Aspen Center for Physics and the Department of Physics at the University of Michigan for hospitality, and acknowledge support from NSF grant AST507428. MW acknowledges support from NASA and EE acknowledges support from NSF grant AST-0206154.

REFERENCES

- Abell, G.O., 1958, ApJS 3,211
- Barkhouse, W.A., et al, 2006, ApJ, 645, 955
- Bernardi, M., Hyde, J.B., Sheth, R.K., Miller, C.J., Nichol, R.C., 2007, AJ 133, 1741
- Blindert, K., Yee, H. K. C., Gladders, M. D., & Ellingson, E. 2004, IAU Colloq. 195: Outskirts of Galaxy Clusters: Intense Life in the Suburbs, 215
- Blindert et al, 2007, to appear
- Bower, R., Lucey, J.R., & Ellis, R.S., 1992, MNRAS, 254, 601
- Bruzual, G., Charlot, S., 2003, MNRAS 344, 1000
- Croton et al, 2006, MNRAS 365, 11
- Dai, X., Kochanek, C.S., Morgan, N.D., 2007, ApJ 658, 917
- Dalton, G.B., Efstathiou, G., Maddox, S.J., & Sutherland, W.J., 1992, ApJL 390, L1
- Davis M., Efstathiou G., Frenk C.S., White S.D.M., 1985, ApJ, 292, 371
- De Lucia, G., et al, 2004, ApJL 610, 7
- De Lucia, G., to appear, talk at Berkeley Nov. 2006
- De Lucia, G., et al, 2007, MNRAS 374, 809
- Eke, V.R., et al, 2004, MNRAS 348, 866
- Ellingson, E., Lin, H., Yee, H.K.C., Carlberg, R.G., 2001, ApJ 547, 609
- Ellis, R.S., 1997, ARA&A 35, 389
- Gal, R. R., Lubin, L. M., Squires, G. K., 2005, AJ, 129, 1827
- Gal, R.R., 2006, preprint [astro-ph/0601195]
- Gilbank, D.G., Bower, R.G., Castander, F.J., Ziegler, B.L., 2004, MNRAS 348, 551
- Gilbank, D.G., Yee, H.K.C., Ellingson, E., Gladders, M.D., Barrientos, L.F., Blindert, K., 2007, ApJ in press, preprint [arxiv/0705.0782]
- Gladders, M.D., Lopez-Cruz, O., Yee, H.K.C., Kodama, T., 1998, ApJ 501, 571
- Gladders, M.D., Yee, H.K.C., 2000, AJ 120, 2148, see also <http://www.astro.utoronto.ca/~gladders/RCS/>
- Gladders, M.D., Yee, H.K.C., 2005, ApJS 157, 1
- Gladders, M.D., et al, 2007, ApJ 655, 128
- Hicks, A., Ellingson, E., Bautz, M., Yee, H., Gladders, M., 2005, AdSpR 36, 706
- Hicks, A., et al, 2007, to appear
- Kaiser, N., Wilson, G., Luppino, G., Kofman, L., Gioia, I. Metzger, M., Dahle, H., 1998, preprint [astro-ph/9809268]
- Kitzbichler, M.G., White, S.D.M., 2007, MNRAS 376, 2

- Kochanek, C.S., White, M., Huchra, J., Macri, L., Jarrett, T.H., Schneider, S.E., Mader, J., 2003, ApJ 585, 161
- Koester B.P., McKay, T.A., et al, 2007, preprint [astro-ph/0701268]
- Lemson, G. & the Virgo Consortium, 2006, preprint [astro-ph/0608019]
- Lopez-Cruz, O., 1997, PhD thesis, University of Toronto
- Lopez-Cruz, O., Barkhouse, W.A., Yee, H.K.C., 2004, ApJ 614, 679
- Lubin, L.M., Brunner, R., Metzger, M.R., Postman, M., Oke, J.B., 2000, ApJL, 531, 5
- Lumsden, S.L., Nichol, R.C., Collins, C.A., Guzzo, L., 1992, MNRAS 258,1
- Miller, C.J., et al, 2005, AJ 130, 968
- Nakata, F., et al, 2005, MNRAS 357, 1357
- Padmanabhan, N., et al, 2006, preprint [astro-ph/0605302]
- Postman, M., Lubin, L.M., Gunn, J.E., Oke, J.B., Hoessel, J.G., Schneider, D.P., Christensen, J.A., 1996, AJ 111, 615
- Reblinsky, K., & Bartelmann, M., 1999, A & A 345,1
- Reiprich, T.H., Boehringer, H., 2002, ApJ 567, 716
- Rozo, E., Wechsler, R.H., Koester, B.P., Evrard, A.E., McKay, T.A., 2007, preprint [astro-ph/0703574]
- Spergel et al, 2006, preprint [astro-ph/0603449]
- Springel, V., et al, 2005, Nature 435, 629
- Stanek, R., Evrard, A.E., Boehringer, H., Schuecker, P., Nord, B., 2006, ApJ 648, 956
- van Haarlem, M.P., Frenk, C.S., White, S.D.M., 1997, MNRAS, 287, 817
- Weinmann, S.M., van den Bosch, F.C. Yang, X., Mo, H.J., 2006a, astro-ph/0607585, to appear in the proceedings of the XLth Rencontres de Moriond, XXVIth Astrophysics Moriond Meeting: "From dark halos to light", Eds. L.Tresse, S. Maurogordato and J. Tran Thanh Van (Editions Frontieres)
- Weinmann, S.M., van den Bosch, F.C., Yang, X., Mo, H.J., 2006b, MNRAS 373, 1159
- White, R., et al 1999, AJ 118, 2014
- White, M., Kochanek, C.S., 2002, ApJ 574, 24
- Wilson, G., 2006, preprint [astro-ph/0604289], <http://spider.ipac.caltech.edu/staff/gillian/SpARCS>
- Yan, R., White, M., Coil, A.L., 2004, ApJ 607, 739
- Yang X., Mo H.J., van den Bosch F.C., Jing Y.P., 2005, MNRAS, 356, 1293
- Yee, H.K.C., Ellingson, E., 2003, Apj 585, 215